# Research Article

Kirti Sharma, Atul Sharma, Mohit Sanduja, Vikas Jogpal, Asim Kumar Mishra\*, Girish Kumar, Tarun Virmani\*, Omar M. Noman, Abdulsalam Alhalmi

# Exploring novel antitubercular agents: Innovative design of 2,3-diaryl-quinoxalines targeting DprE1 for effective tuberculosis treatment

https://doi.org/10.1515/chem-2024-0086 received April 18, 2024; accepted August 10, 2024

**Abstract:** The rising instances of drug resistance in *Mycobacterium tuberculosis* strains pose a significant global health challenge. Conventional tuberculosis (TB) treatments, which typically involve multiple antibiotics, face hurdles like drug resistance, reduced effectiveness, and heightened toxicity. Consequently, there is a pressing need for innovative anti-TB agents with new modes of action. Decaprenyl-phosphoryl-β-D-ribose 2'-epimerase 1(DprE1), a crucial enzyme in *Mycobacterium tuberculosis*, plays a vital role in cell wall biosynthesis – a critical aspect for the bacterium's survival.

\* Corresponding author: Asim Kumar Mishra, Department of Pharmaceutical Chemistry, Amity Institute of Pharmacy, Amity University, Gurugram, Haryana, 122051, India, e-mail: akumar13@ggn.amity.edu

\* Corresponding author: Tarun Virmani, Amity Institute of Pharmacy, Amity University, Greater Noida, UP-201308, India,

e-mail: tarun2feb@gmail.com

**Kirti Sharma:** Department of Pharmaceutical Chemistry, Amity Institute of Pharmacy, Amity University, Gurugram, Haryana, 122051, India; BDM College of Pharmacy, Chhuchhakwas, Jhajjar, 124106, India, e-mail: sharmakirti260@gmail.com

**Atul Sharma:** Department of Pharmaceutical Chemistry, School of Pharmacy, SGT University, Gurugram, India,

e-mail: a.sharmard@gmail.com

**Mohit Sanduja:** School of Pharmacy & Research, Dev Bhoomi Uttarakhand University, Dehradun, 248007, India,

e-mail: drmohitsanduja@gmail.com

Vikas Jogpal: BDM College of Pharmacy, Chhuchhakwas, Jhajjar, 124106, India, e-mail: rxvikasjogpal@gmail.com

**Girish Kumar:** Amity Institute of Pharmacy, Amity University, Greater Noida, UP-201308, India, e-mail: girishmittal89@gmail.com

**Omar M. Noman:** Department of Pharmacognosy, College of Pharmacy, King Saud University, P.O. Box 2457, Riyadh, 11451, Saudi Arabia, e-mail: onoman@ksu.edu.sa

**Abdulsalam Alhalmi:** Department of Pharmaceutics, School of Pharmaceutical Education and Research, Jamia Hamdard, New Delhi, 110062, India, e-mail: asalamahmed5@gmail.com

Building on the success of diarylquinolines like bedaquiline, targeting DprE1 presents a promising avenue for developing anti-TB drugs, especially against drug-resistant strains. Our research focused on discovering novel DprE1 inhibitors using a ligand-based drug design strategy, starting with the established non-covalent inhibitor Ty38c. We assembled a library of 16 molecules, modifying them based on factors like druglike properties, chemical accessibility, and synthetic feasibility. Molecular docking analyses of this library identified three molecules with binding affinities comparable to Ty38c. Among these, KS QD 05 and KS QD 04 are promising candidates, which were further validated through molecular dynamics simulation studies where root-mean-square deviation (RMSD) values of all three complexes reached a plateau, measuring around 0.3 nm, indicating that the apoprotein and all complexes stabilized during the simulation. The ligands KS\_QD\_04 and KS\_QD\_05 displayed significantly stable deviation. KS\_QD\_05 reached about 0.1 nm equilibrium value. However, the ligand KS\_QD\_04 reached an RMSD value of 0.17 nm and showed distress at 70 nm. KS QD 04 and KS\_QD\_05 showed an average value of 1-3 H-bond interaction and regarding the RMSF values, both the compounds showed fluctuations less than 0.5 nm in the case of Mtb. DprE1 enzyme. This indicates the potential of both compounds to become lead compounds in the pursuit of DprE1 inhibitors for TB treatment.

**Keywords:** DprE1, Ty38c, root mean square deviation, root mean square fluctuation, quinoxalines, hydrophobic interactions

# 1 Introduction

Tuberculosis (TB), a highly infectious disease caused by *Mycobacterium tuberculosis*, primarily affects the lungs but can also target other body parts. Despite being one of the oldest known human diseases, TB remains a significant

global health issue, especially in developing countries [1]. According to the World Tuberculosis Report 2022, there were approximately 10.6 million TB cases globally in 2021, a 4.5% increase from the previous year. Tragically, 1.6 million people succumbed to this disease during the same period [2]. TB spreads through the air when an infected person coughs or sneezes, making it highly contagious. The bacteria can remain dormant in the body for years, known as latent TB, and can become active if the immune system weakens.

The standard TB treatment involves a combination of antibiotics over an extended period to ensure complete eradication of the bacteria. However, the emergence of drug-resistant strains, such as multidrug-resistant TB and extensively drug-resistant TB (XDR-TB), poses a significant challenge to global TB control efforts [3]. This situation underscores the urgent need for novel antitubercular agents with new mechanisms of action.

One promising target in TB drug research is decaprenyl-phosphoryl- $\beta$ -D-ribose 2'-epimerase 1 (DprE1), an enzyme involved in the biosynthesis of the Mycobacterium TB cell wall. Inhibiting DprE1 disrupts cell wall formation, weakening the bacterium and making it more susceptible to the immune system and other drugs [4]. Identifying and developing DprE1 inhibitors have shown considerable promise in antitubercular activity [5].

Our study aimed to design novel DprE1 inhibitors through a ligand-based drug design approach or *in silico* approach [6], leveraging the well-established non-covalent inhibitor Ty38c as a starting point. We curated a library of 16 molecules with chemical modifications guided by druglike properties, chemical accessibility, and synthetic feasibility. Molecular docking analyses identified three molecules with notable binding affinities similar to Ty38c. Among these, KS\_QD\_05 and KS\_QD\_04 emerged as promising candidates, validated through molecular dynamics (MD) simulation studies [7,8], which also provides a potential platform for evaluating the natural products [9,10] reinforcing their potential as lead compounds in developing DprE1 inhibitors for TB treatment.

This research holds the potential to contribute significantly to the development of new drugs with improved efficacy and safety profiles, enhancing the arsenal against TB and potentially overcoming drug-resistant strains.

Quinoxalines are fused ring systems of pyrazine and benzopyrazine moieties (Figure 1) with the molecular formula  $C_8H_6N_2$  [11]. It is a low-melting solid, with a melting point ranging from 29 to 30°C and possesses the ability to dissolve in water and is classified as a weak base, as indicated by its  $pK_a$  value of 0.56 [12]. Quinoxalines are N-heterocyclic compounds that have garnered significant attention in the scientific community due to the distinctive arrangement of the two nitrogen atoms within one of its rings. This structural

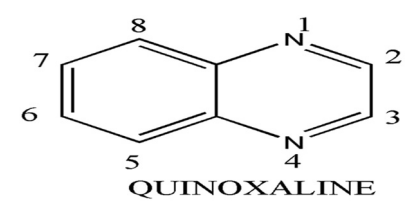


Figure 1: Basic skeleton of quinoxaline.

feature is commonly found in numerous naturally occurring and synthetic compounds, making it a focal point of extensive research efforts [13]. Moreover, the ease of synthesizing quinoxaline derivatives has been a key factor in their broad applications as potential medicinal agents.

Over time, researchers have developed a unique assortment of novel quinoxaline frameworks through the synthesis and evaluation of derivatives featuring various substitutions. These derivatives serve diverse biological functions. By virtue of its distinct electrostatic potential, the quinoxaline molecule exhibits specific hydrophobic and hydrophilic interactions with other molecules, thereby influencing the physicochemical properties observed within the quinoxaline system. Extensive research has been conducted over the past 20 years on the synthesis of quinoxaline, resulting in a comprehensive understanding of these chemical synthetic pathways [11]. A simple yet effective technique for producing quinoxaline is through the condensation reaction of orthophenylenediamine with dicarbonyl compounds, which gives a significant yield. To carry out this method effectively, it is imperative to employ a high temperature, a robust acid catalyst, and extensive heating durations [14]. Recently, there has been a remarkable increase in the application of green methodologies for the synthesis of quinoxalines, including the use of recyclable catalysts [15], one-pot synthesis techniques [16], microwave-assisted synthesis procedures [17,18], and reactions carried out in aqueous solutions [19]. Nowadays, there is a variety of methods available to synthesize quinoxaline derivatives that involve condensation of 1,2-diamines with a-diketones [20], 1,4-addition of 1,2-diamines to diazenylbutenes [21], cyclizatione oxidation of phenacyl bromides [22], and oxidative coupling of epoxides with ene-1,2-diamines [23].

By making slight modifications to the structure of quinoxalines, different molecules are produced that are found to exert remarkable pharmacological efficacy in combating a range of diseases with minimal occurrence of side effects. In regard to this, in the last two decades, several quinoxaline derivatives have been tested for different biological profiles (Figure 2) [24,25]. The most promising activity exhibited by quinoxaline are anti-cancer [26,27], anti-hyperglycemic as PPAR-γ and sulphonyl urea agonists [28], anti-microbial agents [29], anti-convulsant agents [30], anti-fungal agents [31],

Figure 2: Drugs having guinoxaline as the lead moiety.

anti-tubercular agents [32], anti-malarial [33], anti-leishmanial [34], anti-amoebic, anti-HCV [35], anti-inflammatory [36], and anti-viral [37] agents. Most of the authorized medicines contain quinoxaline, demonstrating the scaffolds' adaptability.

In a similar context, the present computational research highlights the potential of substituted 2,3-diaryl quinoxalines and 2-phenyl quinoxalines against DprE1 inhibitors, which can be proven as a potential lead in the discovery of anti-tubercular agents.

# 2 Materials and methods

# 2.1 Molecular docking technique

#### 2.1.1 Protein preparation

PDB ID 4P8K was selected based on its interaction with the enzyme DprE1 [38,39], which allowed the three-dimensional (3D) retrieval of the protein DprE1. The protein was prepared using Glide, a software suite from Schrödinger.

The protein was then subjected to a number of preprocessing procedures, such as bond order assignment, hydrogen removal, and addition, zero-order bond formation to metals, disulphide bond formation, conversion of seleno-methionines to methionines, side chain and loop aided by primers, extraction of water molecules larger than 5 Å from hetero groups, and creation of a HET state with the aid of Epik at pH  $7.0 \pm 2.0$ . After that, the protein was refined using PROPKA at pH 7.0, sampling water orientations to assign H-bonds, and fine-tuning its structure. The protein was further subjected to restrained minimization utilizing the OPLS3 force field, as described in previous studies.

#### 2.1.2 Receptor grid generation

A 20 Å receptor grid was constructed once the protein was prepared. The co-crystallized ligand Ty38c served as the 4 — Kirti Sharma et al. DE GRUYTER

reference point for this grid, which was centred at the active site.

#### 2.1.3 Ligand preparation

The ligands were prepared using Glide, a software suite from Schrödinger.

All of the molecules were built, transformed into 3D structures, and then Maestro's Ligprep and Confgen functions were used to minimize energy. Next, maegz formatting was used to hold the created library.

#### 2.1.4 Molecular docking

After that, molecular docking was carried out to evaluate the interactions between proteins and ligands and ascertain their binding affinities. This was done using the Glide programme and the standard precision (SP) method. The solutions to improve the planarity of the conjugated pi group functions and to incorporate Epik state penalties in the docking scores were selected. The co-crystallized ligand was positioned inside the grid during a re-docking technique to confirm molecular docking; the resultant root-mean-square deviation (RMSD) of 0.197 was considered appropriate for validation.

# 2.2 Molecular dynamic simulation

Using GROMACS 2022.2, an MD simulation was performed. The subsequent procedures were employed.

## 2.2.1 (a) Preparation of the enzyme

The 3D models of the ligand-protein complexes were exported to the .pdb format using Pymol. Simulations were performed to evaluate the dynamic behaviour of the complexes using the GROMACS package software (version 2022.2) [40–42]. pdb2gmx and the CHARMM27 force field were used to build the protein topology. The ligand topology was produced using the SwissParam server [43].

## 2.2.2 (b) System set-up for the simulation

The force field was applied before the complexes were added to the system. With periodic boundary conditions,

they were solvated using the TIP3P water model in a cubic box, which was 1 nm further from the protein border. The Na<sup>+</sup> ions were used to neutralize the system, followed by a 50,000-step phase of energy minimization using the steepest descent approach. Next, 100 ps of a constant-temperature and constant-volume (NVT) simulation at 300 K and 100 ps of NPT simulation were used to bring the system to equilibrium. The components, such as proteins, ligands, water molecules, and ions, were linked independently by the constant-temperature, constant-pressure (NPT) ensemble using the leapfrog approach. The Berendsen temperature and pressure coupling constants were set to 1 and 2. respectively, to maintain the system operative in a stable environment (300 K temperature and 1 bar pressure) [44]. Finally, an MD simulation was run at 300 K for 100 ns in an ensemble under isothermal and isobaric conditions. The bond lengths were restricted using the LINCS approach [45], and the pressure coupling with a time constant was set at 1 ps in order to maintain the pressure at 1 bar. The PME approach [46], which was a part of GROMACS, was used to decrease the error originating from the van der Waals and Coulomb interaction termination at 1.2 nm. To gain insight into the binding free energy, we used the Prime MM-GBSA (molecular mechanics-generalized Born surface area), a method provided by Schrödinger for predicting the free energy of binding of ligands to their target proteins. It combines molecular mechanics energies with continuum solvation models to give a detailed picture of molecular interactions. Prime MM-GBSA is a post-processing method used to calculate the binding free energies based on MD or Monte Carlo simulations. It is often employed in drug discovery for ranking ligands based on their predicted binding affinities to target proteins [47].

The binding free energy ( $\Delta G_{\rm bind}$ ) is calculated using the equation

$$\Delta G_{\text{bind}} = \Delta E_{\text{MM}} + \Delta G_{\text{solv}} + \Delta G_{\text{SA}}$$

where  $\Delta E_{\rm MM}$  is the difference in the molecular mechanic's energy between the complex and sum of the energies of the protein and ligand in their unbound states,  $\Delta G_{\rm solv}$  is the solvation-free energy change upon binding, and  $\Delta G_{\rm SA}$  is the change in the surface area-related non-polar solvation energy upon binding.

#### 2.2.3 (c) Simulation analysis and visualization

Using VMD, trajectory files were shown (Visual MD 1.9.2.) [48] and examined using the locally created HeroMD Analysis programme [49,50] and Xmgrace 5.1.25 [51].

Figure 3: Ligand-based strategy for drug design to design newer substituted 2,3-diaryl-quinoxaline derivatives for inhibiting the DprE1 enzyme.

# 3 Results and discussion

# 3.1 Drug design

A commonly employed method in pharmaceutical research involves "ligand-based drug design," where the objective is to develop new compounds by mimicking the structural and functional features of the established active substances,

known as "ligands." In the pursuit of developing novel substituted 2,3-diaryl-quinoxaline derivatives for inhibiting DprE1, the strategy employed entails initiating the drug discovery process with a well-known ligand, specifically Tyr38c, which is itself a quinoxaline derivative. Tyr38c serves as the foundational compound for the design of these newer substituted derivatives (Figure 3). The improvement of binding affinity, drug-like qualities, chemical availability, and synthesis ease were the main criteria for chemical alterations.

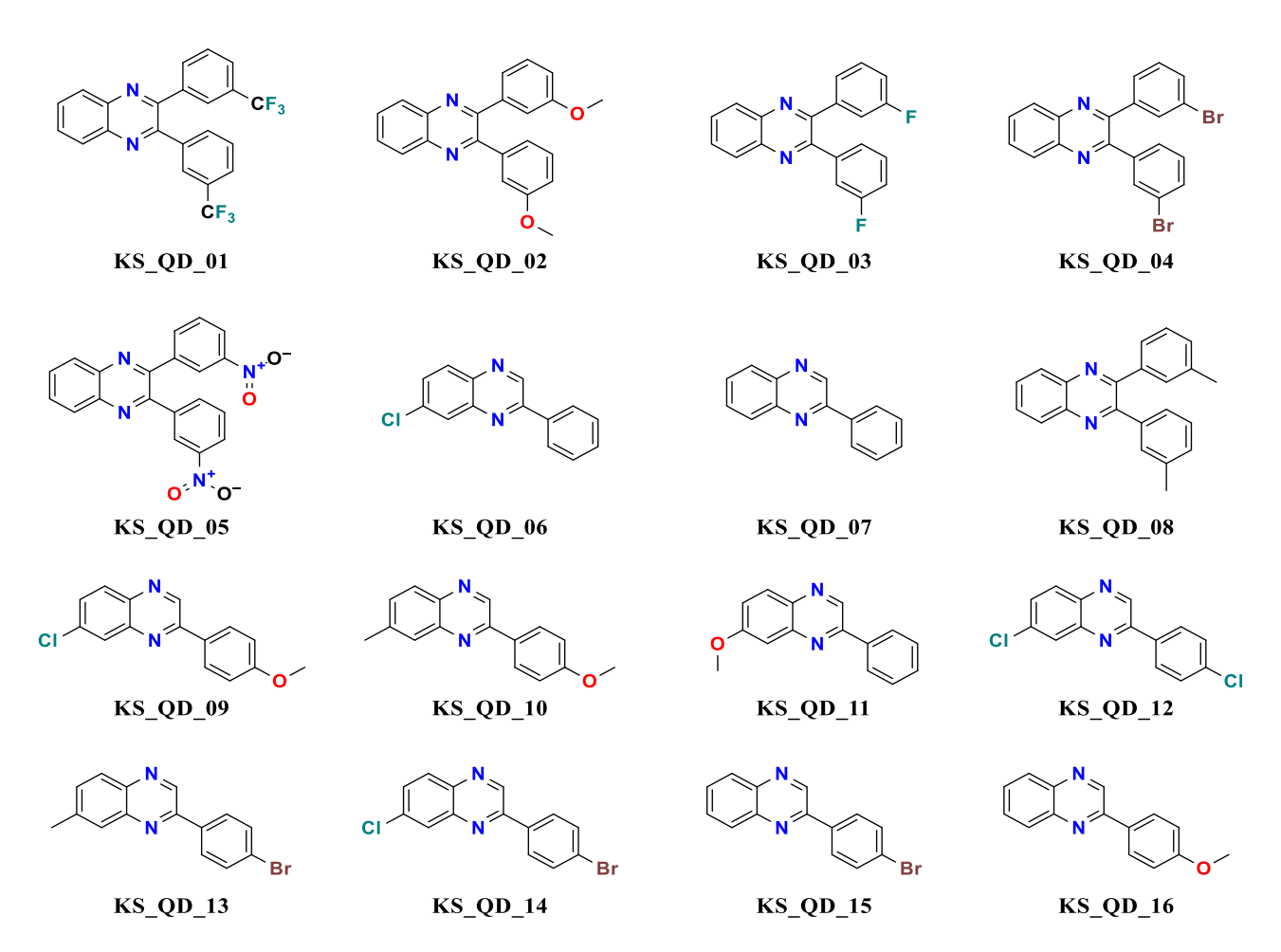


Figure 4: The library of newly designed inhibitors for DprE1, designed around the structure of 2,3-diaryl-quinoxaline derivatives.

6 — Kirti Sharma *et al.* DE GRUYTER

# 3.2 Creating a library of derivatives of 2,3-diaryl-quinoxaline

Based on modifications at different R1 positions at the 2,3-diaryl-quinoxaline and some of the 2-phenyl quinoxaline nucleus based on drug-like properties, availability of chemicals, and their ease of synthesis, a library of 16 molecules was created. The creation of this library of 16 molecules of 2,3-diaryl-quinoxaline derivatives was done carefully based on the principles of medicinal chemistry. The primary objective was to design and synthesize a diverse set of compounds with the potential to inhibit the target enzyme, DprE1, while considering critical factors, such as drug-like properties, chemical availability, and synthetic feasibility. The results are shown in Figure 4.

# 3.3 Molecular docking

The evaluation of molecule binding within the active site of the DprE1 enzyme was conducted using SP docking. A library of 16 molecules, selected based on their synthetic feasibility and drug-like properties, was employed for this analysis. The precision of the approach was first demonstrated via successfully docking the coupled crystal ligand, Ty38c, which replicated the binding posture and orientation seen in the crystal structure. The RMSD value for this validation was 0.197. Subsequently, the same docking protocol was applied to the library of 16 molecules against DprE1. Consequently, three substances have demonstrated high interactions with the catalytic residues found in the DprE1 enzyme's active site. These interactions primarily involved hydrogen bonding and hydrophobic interactions. Among these hits, KS\_QD\_04 and KS\_QD\_05 demonstrated notable binding interactions and were selected for further investigation through MD studies with DprE1 (PDB ID: 4P8K) (Figure 5, Table 1).

# 3.4 DprE1 combined with ligands and as an apoprotein using molecular dynamic simulations, KS\_QD\_04, and KS\_QD\_05

To comprehend conformational changes and assess the molecular binding of KS\_QD\_04 and KS\_QD\_05 against

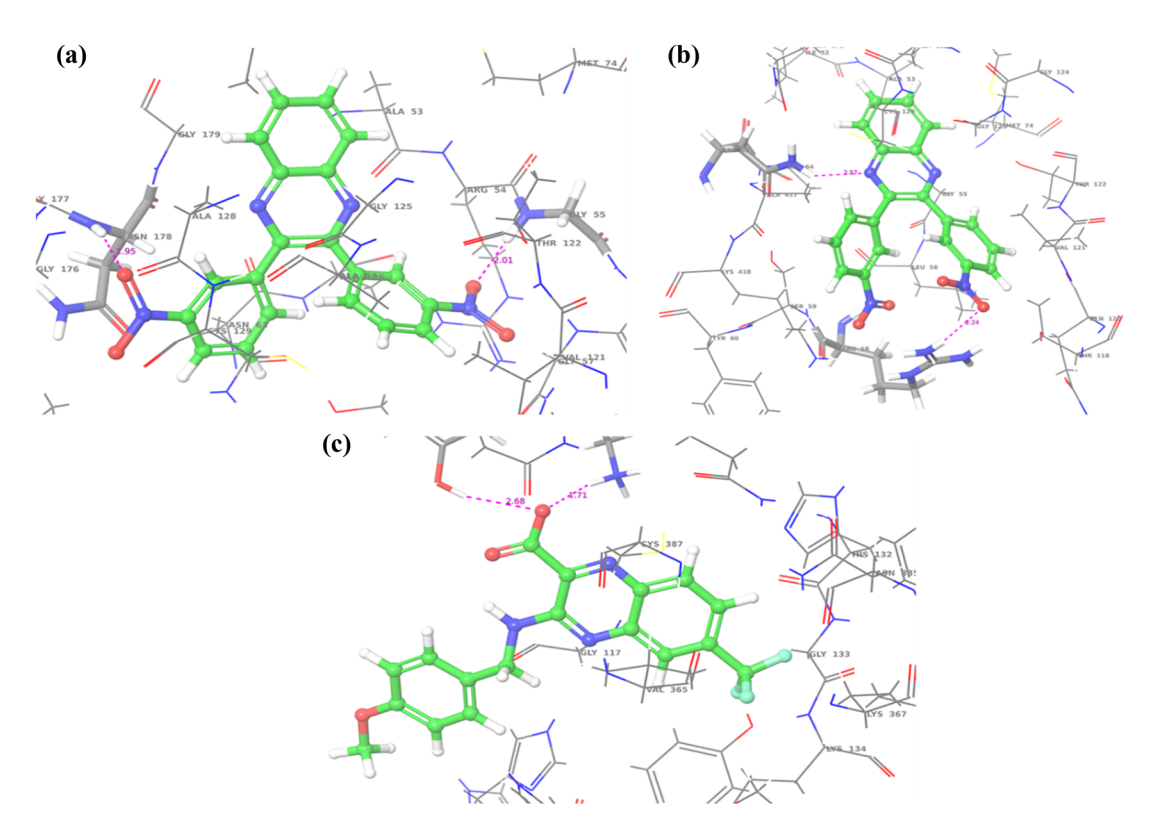


**Figure 5:** Studies of docking indicate orientations at which molecules bind (a) KS\_QD\_05, (b) KS\_QD\_04, and (c) Ty38c in the active site of the DprE1 enzyme. The ligand molecules are depicted as a bold stick representation, with the carbon atoms in green, while the interacting residues within a 4.0 Å radius are shown using stick and wire representations, with the carbon atoms in grey. Hydrogen-bonding interactions are indicated by blue dotted lines, along with the corresponding distances in Å.

Table 1: Studies using molecular docking of different compounds inside the DprE1 active site

S.no	Molecules	Docking score	Model score	Interactions
1.	KS_QD_05	-7.635	-67.223	H-bond interaction with GLY55 and ASN178
2.	KS_QD_04	-7.519	-60.17	H-bond interaction with ARG58 and ASN63; ionic contact with 2X ARG58
3.	KS_QD_03	-7.459	-54.699	H-bond interaction with SER228; pi-stacking interaction with LYS134
4.	KS_QD_06	-6.914	-53.557	Hydrophobic interaction with TYR314, PRO316, LEU317, LEU363, and VAL365
5.	KS_QD_10	-6.613	-47.321	Hydrophobic interaction with PRO316 and LEU317
6.	KS_QD_12	-6.57	-48.996	Hydrophobic interaction with TYR314, PRO316, LEU317, and VAL365
7.	KS_QD_11	-6.549	-46.818	Hydrophobic interaction with TYR314, PRO316, LEU317, and VAL365
8.	KS_QD_01	-6.521	-49.794	Hydrophobic interaction with PHE313, PRO316, LEU317, and VAL365
9.	KS_QD_02	-6.467	-60.917	H-bond interaction with SER228; pi-stacking interaction with LYS134
10.	KS_QD_07	-6.386	-42.785	Hydrophobic interaction with TYR314, LEU315, PRO316, LEU317, and VAL365
11.	KS_QD_09	-6.321	-49.961	Hydrophobic interaction with TYR314, PRO316, LEU317, VAL365, and CYS387
12.	KS_QD_08	-6.307	-45.633	Hydrophobic interaction with TYR314, PRO316, LEU317, and VAL365
13.	KS_QD_16	-6.24	-47.127	Hydrophobic interaction with PRO316, LEU317, and VAL365
14.	KS_QD_14	-5.941	-44.492	Hydrophobic interaction with VAL365, PHE369, and CYS387
15.	KS_QD_13	-5.927	-45.758	Hydrophobic interaction with TYR314, PRO316, VAL365, and CYS387
16.	KS_QD_15	-5.471	-44.513	Hydrophobic interaction with TYR314, PRO316, and VAL365
17.	Ty38c (standard)	-8.210	-80.970	H-bond interaction with TYR60 and LYS418

DprE1, we performed 100 ns of MD simulation on the three models, apoprotein, KS\_QD\_04-Mtb. DprE1, and KS\_QD\_05-Mtb. DprE1 (Figure 6). Several statistical measures, such as hydrogen bond interactions, their % age occupancy, RMSD, and root-mean-square-fluctuation (RMSF), were used to assess their simulations.

#### 3.4.1 RMSD analysis

Analysing the protein-RMSD can help understand any structural alterations to the protein that occur throughout the simulation procedure. Figure 7 shows a temporal multiplot of the protein Ca during three simulations. RMSD

values of all three complexes reached a plateau, measuring around 0.3 nm, indicating that the apoprotein and all complexes stabilized during the simulation [52].

By examining the ligand-RMSD, one can ascertain the stability of the ligand in relation to the protein and binding pocket. The ligand RMSD (nm) against time multiplot for the three simulations is shown in Figure 8. The ligands, KS\_QD\_04, and KS\_QD\_05 have displayed significantly stable deviation. KS QD 05 reached an equilibrium value of about 0.1 nm. However, the ligand KS\_QD\_04 reached an RMSD value of 0.17 nm and showed distress at 70 nm. The RMSD values of the ligand, as observed in the cases, have indicated that all the ligands were capable of binding their respective proteins. RMSD is used to evaluate the stability of the

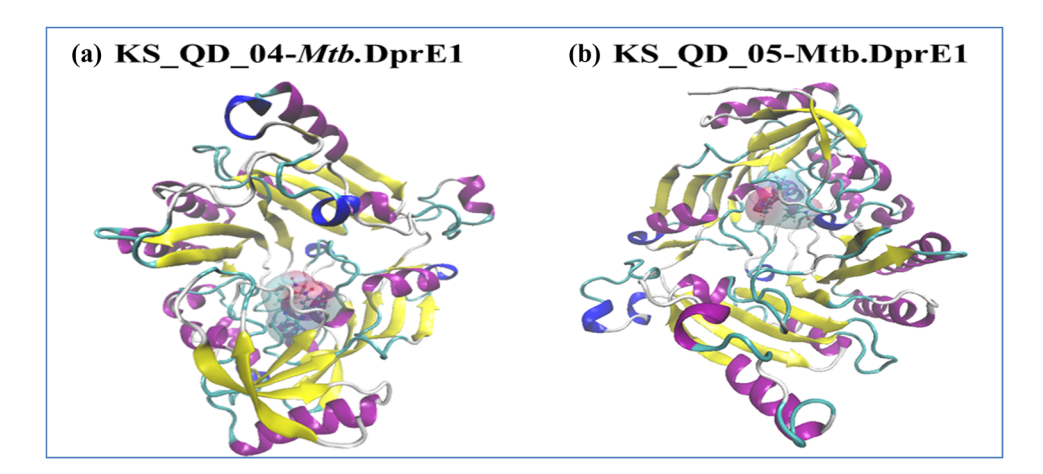


Figure 6: Visual depiction of protein-ligand combinations: (a) KS\_QD\_04-Mtb. DprE1 and (b) KS\_QD\_05-Mtb. DprE1, when the ligand is depicted as a translucent surface in a bond representation and the protein is displayed as a cartoon.

8 — Kirti Sharma et al. DE GRUYTER

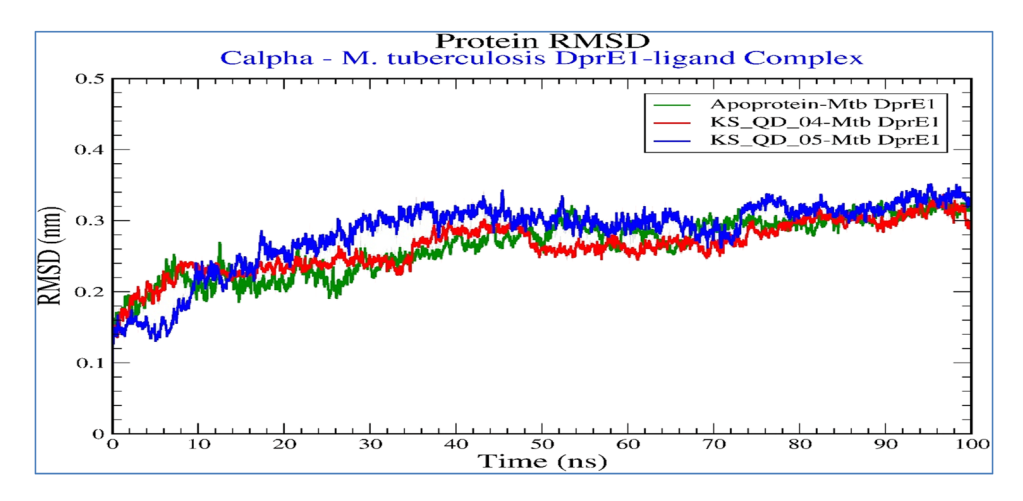


Figure 7: Visual depiction showing protein Cα RMSD (nm) against time (100 nm) for apoprotein (green in colour), KS\_QD\_04-Mtb DprE1 (red in colour), and KS\_QD\_05-Mtb DprE1 (blue in colour) complexes.

protein–ligand complexes during the MD simulations. In this study, the RMSD analysis of the Cα atoms of the apoprotein and its complexes with the ligands KS\_QD\_04 and KS\_QD\_05 indicates that the structures were stable throughout the simulation period. This stability suggests that the binding of the ligands did not induce significant conformational changes in the protein structure, maintaining the overall structural integrity of the DprE1 enzyme.

# 3.4.2 RMSF analysis

Protein-RMSF may be used to characterize the changes at specific locations throughout the protein chain. The multiplot of protein-RMSF (nm) vs the residue number index is shown in Figure 9(a). The plot shows fluctuations less than 0.5 nm in the case of the *Mtb*. DprE1 enzyme when in an

apoprotein form and also in complex with KS\_QD\_04 and KS\_QD\_05. It can be concluded that ligand binding brings stability to the conformation of the protein. The RMSF measures the flexibility of individual residues within the protein structure. RMSF analysis reveals the fluctuation values for the Mtb DprE1 enzyme, both in its apoprotein form and in complex with KS\_QD\_04 and KS\_QD\_05. This indicates that the binding of these ligands contributes to the stabilization of the protein structure, reducing the flexibility of the residues and thus possibly enhancing the binding efficacy and specificity of the inhibitors.

#### 3.4.3 H-bond interaction

Molecular interactions, especially those involving hydrogen bonds, are dependent on both distance and angle, and they

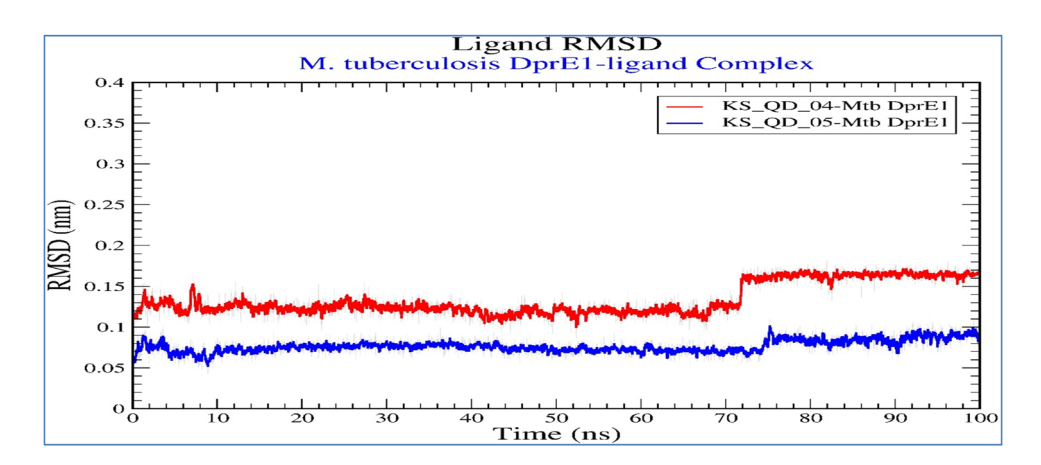


**Figure 8:** An illustration of the graphs displaying RMSD (nm) against time (100 ns) for apoprotein (green colour), KS\_QD\_04-Mtb DprE1 (red in colour), and KS\_QD\_05-Mtb DprE1 (blue in colour) complexes.

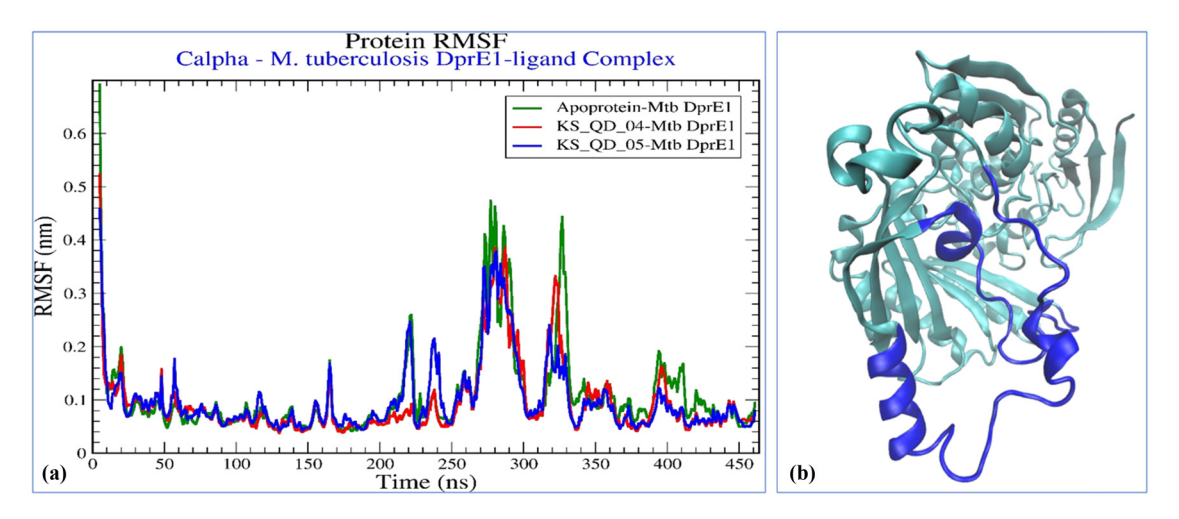


**Figure 9:** (a) Plots displaying RMSF (nm) of the protein against its residue index number are graphically shown for apoprotein (green colour), KS\_QD\_04-Mtb DprE1 (red in colour), and KS\_QD\_05-Mtb DprE1 (blue colour) complexes. (b) The region of the protein that has the greatest RMSF fluctuation (shown in blue).

can break down in dynamic environments. In this section, we have investigated the ligand–protein interactions for each complex. Figure 10 shows the plot of hydrogen number against time. During the course of simulations, KS\_QD\_04 and KS\_QD\_05 showed an average value of 1–3 H-bond interaction. To determine which residues are involved in this type of interaction and their respective stabilities, the percentage of occupancies compared to the residues was also calculated.

The % occupancies of the H-bond connections formed by the two ligands are displayed as a histogram in Figure 11. Figure 11a illustrates the ability of the ligand KS\_QD\_04 to establish stable interactions with DprE1 residues THR118 and ASN63, with occupancies of 6.83 and 6.54%, respectively. On the other hand, the ligand KS\_QD\_05 displayed significant

hydrogen-bond interactions with residues ARG58, GLY57, and ASN178, which remained stable for 12.78, 8.55, and 5.39% of the simulation duration, respectively (Figure 11b). In summary, both ligands exhibit the potential to bind to Mtb DprE1, but KS\_QD\_05 appears to be the most efficient ligand. Hydrogen-bond interactions play a crucial role in the stability and specificity of protein–ligand binding. The occupancy of these hydrogen bonds over the simulation period was also assessed, revealing that the ligand KS\_QD\_04 formed stable interactions with residues THR118 and ASN63 with occupancies of 6.83 and 6.54%, respectively. On the other hand, KS\_QD\_05 exhibited more significant hydrogen-bond interactions with residues ARG58, GLY57, and ASN178, with occupancies of 12.78, 8.55, and 5.39%, respectively. These data indicate that KS\_QD\_05 has a higher potential for stable binding with

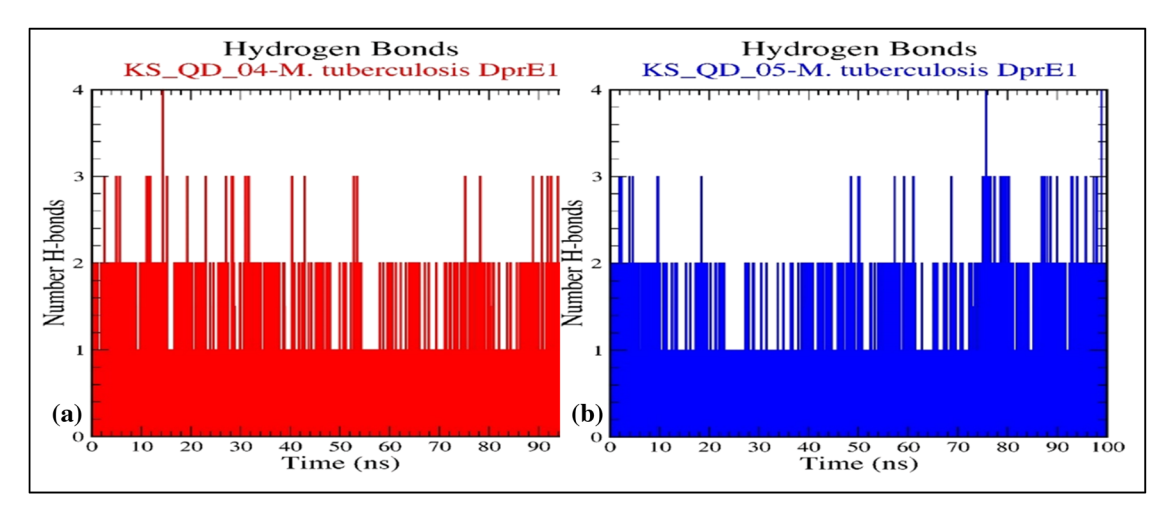
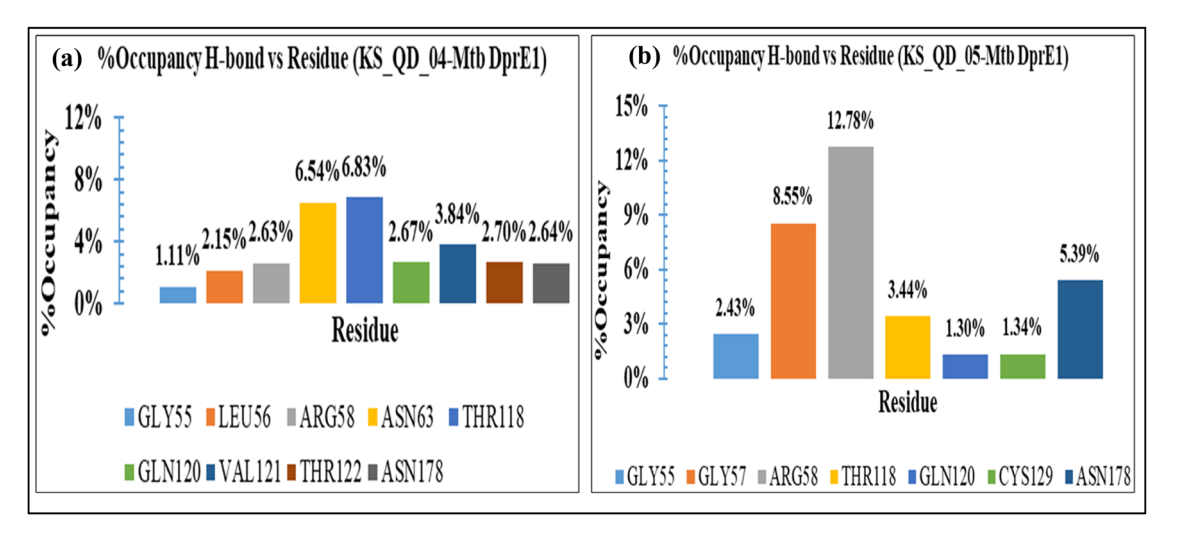


Figure 10: Visual depiction of the quantity of H-bond connections: (a) KS\_QD\_04 (red colour) and (b) KS\_QD\_05 with Mtb. DprE1.



**Figure 11:** A histogram showing the percentage of H-bond protein–ligand interactions that are occupied for (a) KS\_QD\_04 and (b) KS\_QD\_05 in complex with *Mtb*. DprE1.

the DprE1 enzyme, making it a more effective ligand compared to KS\_QD\_04.

The fluctuations observed in the residues ASP268 to GLY301 and ASN309 to GLY331 in the Mtb enzyme DprE1 can be attributed to the inherent flexibility of these regions. Specifically, ASP268 to GLY301 corresponds to a loop region, which naturally exhibits higher mobility, resulting in fluctuations up to 0.5 nm. Similarly, the region from ASN309 to GLY331 contains both a small helix and a loop, contributing to fluctuations up to 0.45 nm. It is important to note that these fluctuating regions do not participate in direct interactions with the ligand. Our structural analysis, using the high-resolution crystal structure of M. TB DprE1 in complex with the non-covalent inhibitor Ty38c (PDB ID 4P8K, resolution: 2.49 Å) confirms that the binding site is distinct and remains stable despite the mobility in these adjacent regions. Therefore, the observed fluctuations in the loop and small helix regions do not adversely affect the overall stability of the ligand-protein complex, ensuring the integrity and reliability of our binding analysis.

#### 3.4.4 In silico ADMET studies

Swiss ADME software was used to perform the *in silico* ADMET studies [53,54]. All molecules in the KS\_QD series have low gastrointestinal (GI) absorption. This indicates that these compounds may not be effectively absorbed through the GI tract when administered orally. None of the molecules are able to permeate the blood–brain barrier (BBB). This is significant for drug design, as it suggests that these compounds are unlikely to affect the central nervous

system (CNS), which can be beneficial if the side effects of CNS are to be avoided. All of the molecules are substrates for P-glycoprotein. Pgp is a transporter protein that pumps foreign substances out of the cells. Being a Pgp substrate may affect the distribution and excretion of these molecules, potentially leading to drug resistance or reduced efficacy. All of the molecules inhibit CYP1A2, CYP2C19, CYP2D6, and CYP3A4. These enzymes are crucial for drug metabolism:

- CYP1A2: Inhibition can affect the metabolism of drugs like caffeine and theophylline.
- CYP2C19: Inhibition can impact the metabolism of drugs such as omeprazole and clopidogrel.
- CYP2D6: Inhibition can interfere with the metabolism of drugs like codeine and beta-blockers.
- CYP3A4: Inhibition can affect the metabolism of a wide range of drugs, including statins and some antiretrovirals.

The KS\_QD series of molecules demonstrate low oral bioavailability due to poor GI absorption and are not suitable for CNS-targeted therapies due to their inability to cross the BBB. They are substrates for P-glycoprotein, which may influence their distribution and elimination. The broad inhibition of CYP enzymes indicates a high potential for drug-drug interactions, which is important for their therapeutic use. Low skin permeability further restricts their administration routes. These factors should be carefully considered in the development and clinical application of these compounds (Table 2).

Drug-likeness results were obtained using Swiss ADME software. All 16 compounds have the same pattern of violations across the different rules (Lipinski, Ghose, Egan, and Muegge) and share the same bioavailability score. The

Table 2: In silico ADMET studies of the proposed drug molecules

Molecule	GI absorption	BBB permeant	Pgp substrate	CYP1 2 inhibitor	CYP2C19 inhibitor	CYP2C9 inhibitor	CYP2D6 inhibitor	CYP3A4 inhibitor	log <i>K</i> p (cm/s)
KS_QD_01	Low	No	Yes	Yes	Yes	No	Yes	Yes	-4.38
KS_QD_02	Low	No	Yes	Yes	Yes	No	Yes	Yes	-4.38
KS_QD_03	Low	No	Yes	Yes	Yes	No	Yes	Yes	-4.38
KS_QD_04	Low	No	Yes	Yes	Yes	No	Yes	Yes	-4.38
KS_QD_05	Low	No	Yes	Yes	Yes	No	Yes	Yes	-4.38
KS_QD_06	Low	No	Yes	Yes	Yes	No	Yes	Yes	-4.38
KS_QD_07	Low	No	Yes	Yes	Yes	No	Yes	Yes	-4.38
KS_QD_08	Low	No	Yes	Yes	Yes	No	Yes	Yes	-4.38
KS_QD_09	Low	No	Yes	Yes	Yes	No	Yes	Yes	-4.38
KS_QD_10	Low	No	Yes	Yes	Yes	No	Yes	Yes	-4.38
KS_QD_11	Low	No	Yes	Yes	Yes	No	Yes	Yes	-4.38
KS_QD_12	Low	No	Yes	Yes	Yes	No	Yes	Yes	-4.38
KS_QD_13	Low	No	Yes	Yes	Yes	No	Yes	Yes	-4.38
KS_QD_14	Low	No	Yes	Yes	Yes	No	Yes	Yes	-4.38
KS_QD_15	Low	No	Yes	Yes	Yes	No	Yes	Yes	-4.38
KS_QD_16	Low	No	Yes	Yes	Yes	No	Yes	Yes	-4.38

single violations in Lipinski, Ghose, Egan, and Muegge's rules suggest that while these compounds might have certain properties that deviate from the optimal ranges, they still retain a moderate probability of bioavailability (0.55). The absence of violations in the Veber rule indicates favourable properties for oral bioavailability in terms of rotatable bonds and polar surface area.

These findings suggest that while the compounds might need some optimization to fully align with all drug-likeness criteria, they possess a reasonable probability of being bioavailable, warranting further investigation and development (Table 3). PAINS (pan-assay interference compounds) alerts indicate the presence of substructures that are likely to interfere with various biological assays, leading to false positives. All of the molecules listed (KS\_QD\_01 to KS\_QD\_16) have a PAINS alert value of 0. This indicates that none of the molecules have substructures that are likely to cause assay interference, which is a positive indicator of their potential as drug candidates. Brenk alerts identify substructures that are problematic in drug development due to toxicity, reactivity, or poor pharmacokinetics. All the molecules listed have a Brenk #alert value of 0. This indicates that none of the molecules contain substructures that are flagged as problematic

Table 3: Drug-likeness results for the proposed drug molecules

Molecule	Lipinski #violations	Ghose #violations	Veber #violations	Egan #violations	Muegge #violations	Bioavailability score
KS_QD_01	1	1	0	1	1	0.55
KS_QD_02	1	1	0	1	1	0.55
KS_QD_03	1	1	0	1	1	0.55
KS_QD_04	1	1	0	1	1	0.55
KS_QD_05	1	1	0	1	1	0.55
KS_QD_06	1	1	0	1	1	0.55
KS_QD_07	1	1	0	1	1	0.55
KS_QD_08	1	1	0	1	1	0.55
KS_QD_09	1	1	0	1	1	0.55
KS_QD_10	1	1	0	1	1	0.55
KS_QD_11	1	1	0	1	1	0.55
KS_QD_12	1	1	0	1	1	0.55
KS_QD_13	1	1	0	1	1	0.55
KS_QD_14	1	1	0	1	1	0.55
KS_QD_15	1	1	0	1	1	0.55
KS_QD_16	1	1	0	1	1	0.55

Table 4: Synthetic accessibility of the proposed drug molecules

Molecule	PAINS #alerts	Brenk #alerts	Leadlikeness #violations	Synthetic accessibility
KS_QD_01	0	0	2	2.97
KS_QD_02	0	0	2	2.97
KS_QD_03	0	0	2	2.97
KS_QD_04	0	0	2	2.97
KS_QD_05	0	0	2	2.97
KS_QD_06	0	0	2	2.97
KS_QD_07	0	0	2	2.97
KS_QD_08	0	0	2	2.97
KS_QD_09	0	0	2	2.97
KS_QD_10	0	0	2	2.97
KS_QD_11	0	0	2	2.97
KS_QD_12	0	0	2	2.97
KS_QD_13	0	0	2	2.97
KS_QD_14	0	0	2	2.97
KS_QD_15	0	0	2	2.97
KS_QD_16	0	0	2	2.97

by this criterion, further supporting their potential suitability as drug candidates. Leadlikeness refers to the properties that make a molecule suitable as a lead compound in drug discovery. The criteria typically include molecular weight, log P (octanol-water partition coefficient), and the number of hydrogen-bond donors and acceptors. All of the molecules have two violations of leadlikeness criteria. While the specific criteria violated are not provided, this suggests that the molecules may have properties slightly outside the ideal range for lead compounds. However, having only two violations is relatively minor and does not necessarily preclude these molecules from being good starting points for drug development. This metric, typically on a scale from 1 (very easy to synthesize) to 10 (very difficult to synthesize), indicates how challenging it is to chemically synthesize the molecules. All the molecules have a synthetic accessibility score of 2.97. This score suggests that the molecules are relatively easy to synthesize, which is advantageous in drug development as it allows for easier production and modification of the compounds (Table 4).

Molecules KS\_QD\_01 to KS\_QD\_16 show promising characteristics as potential drug candidates. These molecules do not have substructures that would typically cause false positives in assays or pose significant risks in terms of toxicity or reactivity. While there are two violations for each molecule, this is not a major issue and can be addressed through further optimization. The ease of synthesis for these molecules makes them attractive candidates for further development and testing. In conclusion, these molecules present a strong foundation for further investigation and optimization in the context of drug discovery, particularly for their

intended application as DprE1 inhibitors for antitubercular activity.

## 3.4.5 Structure-activity relationship

Molecular docking studies identified KS\_QD\_04 and KS\_QD\_05 as the most promising compounds with high binding affinities to the DprE1 enzyme. Notably, KS\_QD\_05 demonstrated significant hydrogen-bond interactions with ARG58, GLY57, and ASN178, with occupancies of 12.78, 8.55, and 5.39%, respectively. The SAR analysis is detailed as follows:

- Hydrophobic and hydrogen bonding interactions: The binding affinity of the inhibitors is strongly influenced by the presence of hydrophobic interactions and hydrogen bonds. KS\_QD\_05 exhibited notably strong and stable hydrogen bonds, which are critical for effective inhibition. This suggests that enhancing these interactions can lead to more potent inhibitors.
- Structural features: The binding affinity is significantly
  affected by the substituents at specific positions of the
  2,3-diaryl-quinoxaline nucleus. For example, the presence
  of hydrophobic groups and hydrogen bond donors/acceptors at positions interacting with GLY55 and ASN178 (for
  KS\_QD\_05), and ARG58 and ASN63 (for KS\_QD\_04) contributes to improved binding.
- 3. Stability in the binding pocket: KS\_QD\_05 demonstrated superior stability within the binding pocket, as indicated by lower RMSD values, suggesting it is a more promising lead compound. The stability highlights the importance of hydrophobic interactions and hydrogen bonding in the inhibitory activity of substituted 2,3-diaryl-quinoxalines against DprE1.

The SAR analysis, supported by molecular docking and MD simulations, underscores the crucial role of hydrophobic interactions and hydrogen bonding in the inhibitory activity of substituted 2,3-diaryl-quinoxalines against DprE1. KS\_QD\_05, with its strong and stable interactions, emerges as the most promising candidate for further development as a DprE1 inhibitor. Future research should aim at optimizing these interactions to enhance both potency and selectivity.

# 4 Conclusions

The study focused on identifying novel DprE1 inhibitors as potential anti-TB agents using a ligand-based drug design approach. A library of 16 substituted 2,3-diaryl-quinoxaline

derivatives was designed and evaluated through molecular docking and MD simulations. Protein stability is evaluated by the RMSD analysis, which showed that both the apoprotein and protein-ligand complexes reached a stable plateau around 0.3 nm, indicating structural stability during the 100 ns simulation. The ligand RMSD plots demonstrated that both KS\_QD\_04 and KS\_QD\_05 maintained relatively stable interactions with DprE1. KS QD 05 achieved an equilibrium RMSD of about 0.1 nm, while KS QD 04 showed some disturbance around 70 ns but stabilized at 0.17 nm. RMSF analysis revealed fluctuations less than 0.5 nm for both the apoprotein and ligand-bound complexes, suggesting that ligand binding contributed to protein conformational stability, which established the protein stability. Both ligands formed an average of 1-3 hydrogen bonds throughout the simulation. KS\_QD\_04 formed stable interactions with THR118 (6.83% occupancy) and ASN63 (6.54% occupancy). KS QD 05 showed more significant hydrogen bonding with ARG58 (12.78% occupancy), GLY57 (8.55% occupancy), and ASN178 (5.39% occupancy). In conclusion, the MD simulations support the potential of both KS QD 04 and KS QD 05 as DprE1 inhibitors. However, KS\_QD\_05 demonstrated more stable and extensive hydrogen bonding interactions, suggesting it may be a more promising candidate for further development as an anti-TB agent. These findings provide a solid foundation for future experimental validation and optimization of these compounds in the ongoing search for effective treatments against drug-resistant tuberculosis.

**DE GRUYTER** 

**Acknowledgments:** The authors extend their appreciation to Researchers Supporting Project number (RSPD2024R1087), King Saud University, Riyadh, Saudi Arabia, for funding this work.

**Funding information:** This research was funded by Researchers Supporting Project number (RSPD2024R1087), King Saud University, Riyadh, Saudi Arabia.

Author contributions: Conceptualization, K.S. and A.S.; methodology, K.S.; software, M.S.; validation, V.J., A.K.M. and A.A.; formal analysis, G.K. and A.A; investigation, T.V.; resources, G.K.; data curation, O.M.N.; writing - original draft preparation, K.S.; writing – review and editing, A.S., M.S., V.J., G.K., T.V., O.M.N., and A.A.; visualization, T.V.; supervision, A.K.M.; project administration and funding acquisition, O.M.N. All authors have read and agreed to the published version of the manuscript.

Conflict of interest: The authors declare no conflicts of interest.

Data availability statement: Data of this research are available upon request from the corresponding authors.

# References

- Lawn SD, Zumla AI. Tuberculosis. Lancet. 2011 Jul;378(9785):57-72. [1]
- Kumar M, Virmani T, Kumar G, Deshmukh R, Sharma A, Duarte S, [2] et al. Nanocarriers in tuberculosis treatment: challenges and delivery strategies. Pharmaceuticals. 2023;16(10):1360.
- WHO. Global Tuberculosis Report 2022 [Internet]. [cited 2024 Mar 281. Available from https://www.who.int/teams/globaltuberculosis-programme/tb-reports/global-tuberculosisreport-2022.
- Dean AS, Auguet OT, Glaziou P, Zignol M, Ismail N, Kasaeva T, et al. 25 years of surveillance of drug-resistant tuberculosis: achievements, challenges, and way forward. Lancet Infect Dis. 2022;22(7):e191-6.
- Ahalwat S, Bhatt DC, Rohilla S, Jogpal V, Sharma K, Virmani T, et al. [5] Mannose-functionalized isoniazid-loaded nanostructured lipid carriers for pulmonary delivery: in vitro prospects and in vivo therapeutic efficacy assessment. Pharmaceuticals. 2023;16(8):1108.
- Neto RD, Santos CB, Henriques SV, Machado LD, Cruz JN, da Silva CH, et al. Novel chalcones derivatives with potential antineoplastic activity investigated by docking and molecular dynamics simulations. J Biomol Struct Dyn. 2022;40(5):2204-16.
- Silva LB, Ferreira EFB, Maryam, Espejo-Román JM, Costa GV, Cruz JV, et al. Galantamine based novel acetylcholinesterase enzyme inhibitors: a molecular modeling design approach. Molecules. 2023;28:1035. doi: 10.3390/molecules28031035.
- [8] de Almeida RBM, Barbosa DB, do Bomfim MR, Amparo IAO, Andrade BS, Costa SL, et al. Identification of a novel dual inhibitor of acetylcholinesterase and butyrylcholinesterase: in vitro and in silico studies. Pharmaceuticals. 2023;16:95. doi: 10.3390/
- [9] Mesquita KD, Feitosa BD, Cruz IN, Ferreira OO, Franco CD, Cascaes MM, et al. Chemical composition and preliminary toxicity evaluation of the essential oil from peperomia circinnata link var. circinnata. (piperaceae) in artemia salina leach. Molecules. 2021;26:7359. doi: 10.3390/molecules26237359.
- Alves FS, Rodrigues Do Rego JA, Da Costa ML, Lobato Da Silva LF, Da Costa RA, Cruz JN. Spectroscopic methods and in silico analyses using density functional theory to characterize and identify piperine alkaloid crystals isolated from pepper (Piper Nigrum L.). J Biomol Struct Dyn. 2019;38(9):2792-9. doi: 10.1080/07391102.2019. 1639547.
- Vitaku E, Smith DT, Njardarson JT. Analysis of the structural diversity, substitution patterns, and frequency of nitrogen heterocycles among US FDA approved pharmaceuticals: miniperspective. J Med Chem. 2014;57(24):10257-74.
- Khatoon H, Abdulmalek E. Novel synthetic routes to prepare bio-[12] logically active quinoxalines and their derivatives: A synthetic review for the last two decades. Molecules. 2021;26(4):1055.
- Abulkhair HS, Elmeligie S, Ghiaty A, El-Morsy A, Bayoumi AH, Ahmed HEA, et al. In vivo-and in silico-driven identification of novel synthetic quinoxalines as anticonvulsants and AMPA inhibitors. Arch Pharm (Weinh). 2021;354(5):2000449.

- [14] Zayed MF. Medicinal chemistry of quinazolines as anticancer agents targeting tyrosine kinases. Sci Pharm. 2023;91(2):18.
- [15] Niknam K, Saberi D, Mohagheghnejad M. Silica bonded S-sulfonic acid: a recyclable catalyst for the synthesis of quinoxalines at room temperature. Molecules. 2009;14(5):1915–26.
- [16] Thakuria H, Das G. One-pot efficient green synthesis of 1, 4-dihydro-quinoxaline-2, 3-dione derivatives. J Chem Sci. 2006:118:425–8.
- [17] da Costa CF, Nora de Souza MV, Brandao Gomes CR, Facchinetti V. Microwave-assisted synthesis of quinoxalines-A review. Curr Microw Chem. 2017;4(4):277–86.
- [18] Rostamizadeh S, Jafari S. The synthesis of quinoxalines under microwave irradiation. Indian | Heterocycl Chem. 2001;10(4):303–4.
- [19] Arde SM, Patil AD, Mane AH, Salokhe PR, Salunkhe RS. Synthesis of quinoxaline, benzimidazole and pyrazole derivatives under the catalytic influence of biosurfactant-stabilized iron nanoparticles in water. Res Chem Intermed. 2020;46:5069–86.
- [20] Brown DJ. The Chemistry of Heterocyclic Compounds-The Naphthyridines. Hoboken, New Jersey: John Wiley & Sons, Inc; 2022.
- [21] Aparicio D, Attanasi OA, Filippone P, Ignacio R, Lillini S, Mantellini F, et al. Straightforward access to pyrazines, piperazinones, and quinoxalines by reactions of 1, 2-diaza-1, 3-butadienes with 1, 2-diamines under solution, solvent-free, or solid-phase conditions. J Org Chem. 2006;71(16):5897–905.
- [22] Shi D, Dou G, Ni S, Shi J, Li X. An efficient synthesis of quinoxaline derivatives mediated by stannous chloride. ChemInform. 2009;40(15):1797–801.
- [23] Antoniotti S, Duñach E. Direct and catalytic synthesis of quinoxaline derivatives from epoxides and ene-1, 2-diamines. Tetrahedron Lett. 2002;43(22):3971–3.
- [24] Sharma A, Deep A, Marwaha MG, Marwaha RK. Quinoxaline: A chemical moiety with spectrum of interesting biological activities. Mini Rev Med Chem. 2022;22(6):927–48.
- [25] Tariq S, Somakala K, Amir M. Quinoxaline: An insight into the recent pharmacological advances. Eur J Med Chem. 2018;143:542–57.
- [26] Ingle R, Marathe R, Magar D, Patel HM, Surana SJ. Sulphonamidoquinoxalines: Search for anticancer agent. Eur J Med Chem. 2013:65:168–86.
- [27] El Newahie AMS, Ismail NSM, Abou El Ella DA, Abouzid KAM. Quinoxaline-based scaffolds targeting tyrosine kinases and their potential anticancer activity. Arch Pharm (Weinh). 2016;349(5):309–26.
- [28] Ibrahim MK, Eissa IH, Abdallah AE, Metwaly AM, Radwan MM, ElSohly MA. Design, synthesis, molecular modeling and antihyperglycemic evaluation of novel quinoxaline derivatives as potential PPARy and SUR agonists. Bioorg Med Chem. 2017;25(4):1496–513.
- [29] Shintre SA, Ramjugernath D, Islam MS, Mopuri R, Mocktar C, Koorbanally NA. Synthesis, in vitro antimicrobial, antioxidant, and antidiabetic activities of thiazolidine–quinoxaline derivatives with amino acid side chains. Med Chem Res. 2017;26:2141–51.
- [30] El-Helby A-GA, Ayyad RRA, El-Adl K, Elwan A. Quinoxalin-2 (1 H)-one derived AMPA-receptor antagonists: Design, synthesis, molecular docking and anticonvulsant activity. Med Chem Res. 2017;26:2967–84.
- [31] Guillon J, Nim S, Moreau S, Ronga L, Savrimoutou S, Thivet E, et al. Synthesis of new piperazinyl-pyrrolo [1, 2-a] quinoxaline derivatives as inhibitors of Candida albicans multidrug transporters by a

- Buchwald–Hartwig cross-coupling reaction. RSC Adv. 2020:10(5):2915–31.
- [32] Shekhar AC, Rao PS, Narsaiah B, Allanki AD, Sijwali PS. Emergence of pyrido quinoxalines as new family of antimalarial agents. Eur J Med Chem. 2014;77:280–7.
- [33] Cogo J, Kaplum V, Sangi DP, Ueda-Nakamura T, Correa AG, Nakamura CV. Synthesis and biological evaluation of novel 2, 3disubstituted quinoxaline derivatives as antileishmanial and antitrypanosomal agents. Eur J Med Chem. 2015;90:107–23.
- [34] Soto-Sánchez J, Caro-Gómez LA, Paz-González AD, Marchat LA, Rivera G, Moo-Puc R, et al. Biological activity of esters of quinoxaline-7-carboxylate 1, 4-di-N-oxide against E. histolytica and their analysis as potential thioredoxin reductase inhibitors. Parasitol Res. 2020:119:695–711.
- [35] Chakraborty J, Kanungo A, Mahata T, Kumar K, Sharma G, Pal R, et al. Quinoxaline derivatives disrupt the base stacking of hepatitis C virus-internal ribosome entry site RNA: reduce translation and replication. Chem Commun. 2019;55(93):14027–30.
- [36] Shen Q-K, Gong G-H, Li G, Jin M, Cao L-H, Quan Z-S. Discovery and evaluation of novel synthetic 5-alkyl-4-oxo-4, 5-dihydro-[1, 2, 4] triazolo [4, 3-a] quinoxaline-1-carbox-amide derivatives as anti-inflammatory agents. J Enzyme Inhib Med Chem. 2020;35(1):85–95.
- [37] Montana M, Montero V, Khoumeri O, Vanelle P. Quinoxaline derivatives as antiviral agents: a systematic review. Molecules. 2020;25(12):2784.
- [38] Neres J, Hartkoorn RC, Chiarelli LR, Gadupudi R, Pasca MR, Mori G, et al. 2-Carboxyquinoxalines Kill Mycobacterium tuberculosis through Noncovalent Inhibition of DprE1. ACS Chem Biol. 2015;10:705–14.
- [39] Hu XP, Yang L, Chai X, Lei YX, Alam MS, Liu L, et al. Discovery of novel DprE1 inhibitors via computational bioactivity fingerprints and structure-based virtual screening. Acta Pharmacol Sin. 2022 Jun;43(6):1605–15. doi: 10.1038/s41401-021-00779-1, Epub 2021 Oct 19 PMID: 34667293; PMCID: PMC9160271.
- [40] Bekker H, Berendsen HJC, Dijkstra EJ, Achterop S, Vondrumen R, Vanderspoel D, et al. Gromacs-a parallel computer for moleculardynamics simulations. 4th International Conference on Computational Physics (PC 92). World Scientific Publishing; 1993. p. 252–6.
- [41] Ganesan A, Coote ML, Barakat K. Molecular dynamics-driven drug discovery: leaping forward with confidence. Drug Discov Today. 2017;22(2):249–69.
- [42] Thalla M, Kant K, Dalchand, Rawat R, Banerjee S. Merged experimental guided computational strategy toward tuberculosis treatment mediated by alveolar macrophages mannose receptor. J Biomol Struct Dyn. 2020;38(17):5195–203.
- [43] Schmid N, Eichenberger AP, Choutko A, Riniker S, Winger M, Mark AE, et al. Definition and testing of the GROMOS force-field versions 54A7 and 54B7. Eur Biophys J. 2011;40:843–56.
- [44] Van Aalten DMF, Bywater R, Findlay JBC, Hendlich M, Hooft RWW, Vriend G. PRODRG, a program for generating molecular topologies and unique molecular descriptors from coordinates of small molecules. J Comput Aided Mol Des. 1996;10:255–62.
- [45] Berendsen HJC, van der Spoel D, van Drunen R. GROMACS: A message-passing parallel molecular dynamics implementation. Comput Phys Commun. 1995;91(1–3):43–56.
- [46] Di Pierro M, Elber R, Leimkuhler B. A stochastic algorithm for the isobaric–isothermal ensemble with Ewald summations for all long range forces. J Chem Theory Comput. 2015;11(12):5624–37.

- [47] Li J, Abel R, Zhu K, Cao Y, Zhao S, Friesner RA. The VSGB 2.0 model: a next generation energy model for high resolution protein structure modeling. Proteins. 2011;79:2794-812.
- [48] Humphrey W, Dalke A, Schulten K. VMD: visual molecular dynamics. J Mol Graph. 1996;14(1):33-8.
- [49] Rawat R, Kant K, Kumar A, Bhati K, Verma SM. HeroMDAnalysis: an automagical tool for GROMACS-based molecular dynamics simulation analysis. Future Med Chem. 2021;13(5):447-56.
- [50] Devi S, Rangra NK, Rawat R, Alrobaian MM, Alam A, Singh R, et al. Anti-atherogenic effect of Nepitrin-7-O-glucoside: A flavonoid isolated from Nepeta hindostana via acting on PPAR- $\alpha$  receptor. Steroids. 2021;165:108770.
- [51] Vaught A. Graphing with Gnuplot and Xmgr: two graphing packages available under linux. Linux J. 1996;1996(28es):7-es.
- [52] Adnan C. In silico studies on stilbenolignan analogues as SARS-CoV-2 Mpro inhibitors. Chem Phys Lett. May 2021;771:138563.
- [53] Cetin A. Some flavolignans as potent SARS-CoV-2 inhibitors via molecular docking, molecular dynamic simulations and ADME analysis. Curr Comput Aided Drug Des. 2022;18:337-46.
- [54] Seyma Sevincli Z, Bildirici N, Cetin A, Bildirici I. GABA-AT inhibitors: design, synthesis, pharmacological characterization, molecular docking and ADMET studies. ChemistrySelect. 2023;8:1-12. doi: 10. 1002/slct.202302683.